P.H. PIOGER[1]
V. COUDERC[1,✉]
L. LEFORT[1]
A. BARTHÉLÉMY[1]
F. BARONIO[2,*]
C. DE ANGELIS[2]
Y.H. MIN[3]
V. QUIRING[3]
W. SOHLER[3]

# Ultra-fast saturable absorber through spatial self-trapping and filtering in Ti : PPLN film waveguides

[1] I.R.C.O.M., Faculté des Sciences, Université de Limoges/CNRS, 123 Ave. A. Thomas, 87060 Limoges, France
[2] Istituto Nazionale per la Fisica delle materia, Dipartimento di Elettronica per l'Automazione, Università di Brescia, via Branze 38, 25123 Brescia, Italy
[3] Universität Paderborn, Angewandte Physik, 33095 Paderborn, Germany

**ABSTRACT** Numerical and experimental investigations on ultra-fast all-optical saturable absorber on picosecond optical pulses at 1547 nm using spatial self-trapped propagation in a quadratic nonlinear film waveguide combined with spatial filtering are reported. The influences of phase-mismatch, pulse intensity and spatial filtering on the temporal reshaping mechanism are discussed to derive the optimum parameters.

**PACS** 42.65.Ky, 42.65.Re, 42.65.Wi

## 1 Introduction

Self-focusing and self-trapping of light waves have been investigated since the early stages of nonlinear optics. Interest in this field has been maintained by the large variety of fascinating phenomena encountered and their potential applications, such as soliton propagation, all-optical switching, and ultra-fast signal processing. For many years such effects have been investigated using the optical Kerr effect in cubic nonlinear media [1–7]. However, self-induced trapping of light also occurs in quadratic nonlinear media. In this case, spatial, temporal and spatio-temporal solitons are formed by the mutual focusing and trapping of the waves parametrically interacting in the nonlinear medium [8–14]. Spatial solitons exist in particular in the process of second-harmonic generation that is addressed here. They are formed in waveguides and in bulk crystals by mutual trapping of the beams at the fundamental frequency (FF) and at the second-harmonic frequency (SH). Several soliton families exist; they are dynamically stable for all values of the wave-vector mismatch between the interacting waves. In most experimental situations a quadratic soliton is excited by launching only a powerful FF beam. The SH component is formed within a few millimetres of propagation by frequency doubling of the input field.

Because of the high peak powers required to excite quadratic solitons in nonlinear crystals of some centimetre length, solitons are in practice generated using pulsed laser light. Therefore, only the fraction of the pulse exceeding the soliton power threshold propagates in a self-trapped way; the low power parts of the pulse behave linearly and undergo diffraction inside the crystal. An aperture, properly positioned at the output face of the nonlinear medium, may block an appreciable part of the non-trapped energy, but transmits the self-guided beam. So the transmitted pulse mainly contains the high power part of the input pulse and the overall system (nonlinear propagation medium plus spatial filter) acts as a saturable absorber with an ultra-fast response time. The variation and threshold of the intensity dependent transmittance can be adjusted by changing the propagation distance, the input beam width and the output spatial filtering.

In a previous paper, Simos et al. demonstrated the saturable absorber operation of the proposed arrangement at 1064 nm [15]. The 63 ps gaussian pulses from a Q-switched, mode-locked Nd : YAG laser were shortened thanks to the excitation of 2D quadratic solitons in a 2 cm long KTP crystal and their subsequent filtering at the output. In these experiments the group velocity mismatch between the fundamental and the second harmonic was too weak with respect to the pulse duration ($L_{KTP} = 0.1 L_{GVM}$) to influence the behaviour of the device. The aim of the investigations reported below was to determine whether this method could be adapted to the optical communication domain and whether the speed of operation of the spatial soliton based component could go beyond the limit fixed by the group velocity mismatch. The use of short or very short pulses is unfavourable to excite quadratic spatially trapped beams particularly because of the strong group velocity mismatch between the different frequency components required to form the solitary beam. Nevertheless, it was shown numerically and experimentally that with sufficiently large positive phase-mismatch spatial trapping in quadratic media can be maintained even if the pump pulse duration is shorter than the group delay mismatch between FF and SH components [16, 17].

On the basis of these previous results we studied numerically and experimentally the temporal nonlinear absorber mechanism realized by spatial trapping and filtering using picosecond pulses, shorter than the group delay difference between the FF and SH waves; only a FF pulse of 1547 nm wavelength was launched into the device. The influences of input intensity, of phase-mismatch conditions and of the spatial filter diameter on the transmittance of the device have been also studied. The conditions leading to the optimum

✉ Fax: +33-5/5545-7253, E-mail: condercv@ircom.unilim.fr
*Present address: I.N.F.M., Dipartimento di Ingegneria dell'Informazione, Uìversità di Padova, Via Gradenigo 6/b, 35131 Pavova, Italy

pulse reshaping were determined. The experimental study was realised with one dimensional self-trapped propagation in a Ti-indiffused periodically poled LiNbO$_3$ (Ti : PPLN) film waveguide. The high nonlinearity of the waveguide permitted to diminish significantly the intensity required to obtain self-trapping and temporal filtering.

The paper is organized as follows. In Sect. 2 a numerical investigation of the temporal saturable absorber mechanism is shown. In Sect. 3 a report is given on an experimental example of the reshaping mechanism. Finally, in Sect. 4 the main conclusions are drawn.

## 2 Numerical investigation

Initial considerations begin with second harmonic generation with light beams traveling in a medium of large quadratic nonlinearity with periodic sign reversal as in PPLN to get quasi phase matching of nonlinear interactions. The quasi phase matching technique introduces a grating wavevector in the system to compensate for the linear-wave-vector mismatch between the FF and SH waves. Here, we assume first order quasi phase matching and study the propagation in a slab waveguide, but this analysis can be extended to bulk geometries. The electric fields $E_1$ and $E_2$, at fundamental frequency ($\omega_0$) and at second harmonic ($2\omega_0$) respectively, propagating in the $z$ direction, can be written as:

$$E_1(x, y, z, t) = \frac{1}{2}(W(y)w(x, z, t)$$
$$\times \exp\left(-j\left(\beta(\omega_0)z + \omega_0 t\right)\right) + \text{c.c})$$

$$E_2(x, y, z, t) = \frac{1}{2}(V(y)v(x, z, t)$$
$$\times \exp\left(-j\left(\beta(2\omega_0)z + 2\omega_0 t\right)\right) + \text{c.c})$$

$W(y)$ and $V(y)$ are the mode profiles at FF and SH in the guided dimension, $w(x, z, t)$ and $v(x, z, t)$ the slowly varying envelopes. Averaging over the quasi phase matching periods, at the lowest order, $w(x, z, t)$ and $v(x, z, t)$ obey the nonlinear coupled equations [18]:

$$j\frac{\partial w}{\partial z} - j\beta'_{\omega_0}\frac{\partial w}{\partial t} - \frac{\beta''_{\omega_0}}{2}\frac{\partial^2 w}{\partial t^2} + \frac{1}{2\beta_{\omega_0}}\frac{\partial^2 w}{\partial x^2}$$
$$+ \frac{\chi^{(2)}\omega_0}{2cn_{\omega_0}}\frac{\int V|W|^2\,dy}{\int |W|^2\,dy}vw^*e^{-j\Delta kz} = 0$$

$$j\frac{\partial v}{\partial z} - j\beta'_{2\omega_0}\frac{\partial v}{\partial t} - \frac{\beta''_{2\omega_0}}{2}\frac{\partial^2 v}{\partial t^2} + \frac{1}{2\beta_{2\omega_0}}\frac{\partial^2 v}{\partial x^2}$$
$$+ \frac{\chi^{(2)}\omega_0}{2cn_{2\omega_0}}\frac{\int V|W|^2\,dy}{\int |V|^2\,dy}w^2e^{j\Delta kz} = 0 \qquad (1)$$

where $\beta$ represents the propagation constant, $\beta'$ the inverse group velocity, $\beta''$ the inverse group-velocity dispersion; $n$ is the refractive index, $\Delta k = 2\beta_{\omega 0} - \beta_{2\omega 0} + K_S$, where $K_S = 2\pi/\Lambda$, and $\chi^{(2)} = 2/\pi\chi^{(2)}_{z'z'z'}$ is the nonlinear coefficient. We employ a finite-difference vectorial mode solver to determine the linear propagation properties in the slab waveguide; finally, using a finite-difference beam propagation technique, we solve the nonlinear coupled equations (1).

The propagation of FF beams of narrow spots along the waveguide plane (e.g, $w_{ox} = 56\,\mu$m FWHM) is considered, with few picosecond pulsed temporal excitation (e.g., $w_{ot} = 3.9$ ps FWHM), only the FF at the input at 1547 nm, in a Ti : PPLN waveguide of length $L = 58$ mm. Under these conditions, the crystal length corresponds to 5.6 times the FF diffraction length and to 5.4 times the walk-



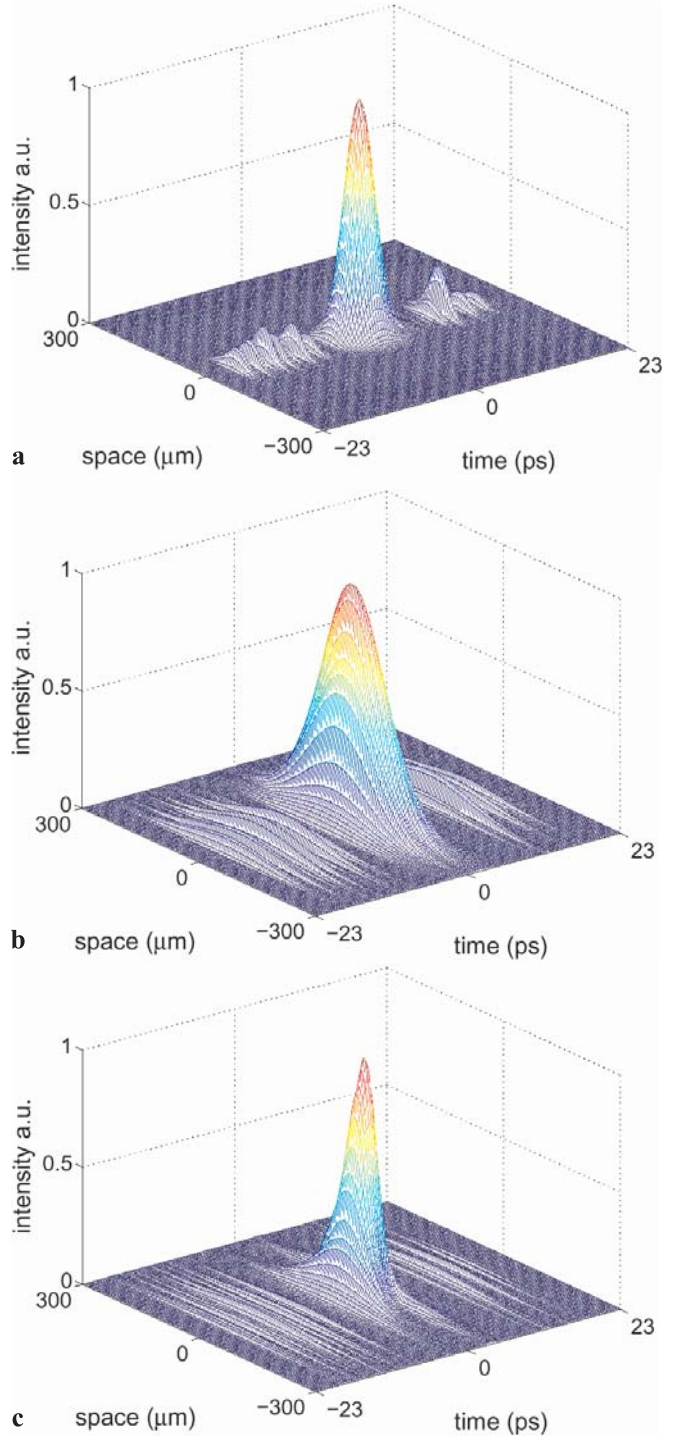**FIGURE 1** FF slowly varying envelope profiles: at the input of the nonlinear medium (**a**); at the output of the nonlinear medium in the low intensity regime (diffraction dominates) (**b**) and in the nonlinear trapped regime (**c**). The phase-mismatch is $\Delta kL \sim 15\pi$; in the low intensity regime $I = 1$ MW/cm$^2$ (peak intensity), in the self-trapped regime $I = 280$ MW/cm$^2$

off length between FF and SH; the dispersive terms can be neglected.

Because of the presence of a large temporal walk off, a spatial self-trapped propagation of few picosecond pulses is obtained only at positive phase-mismatch. The trapping is defined as the equivalence of the output and the input beam size. When spatial trapping occurs, the FF pulse undergoes a moderate temporal self-steepening of the trailing edge, due to the locking with the SH component [17].

Moreover, a main temporal pulse of about 3.9 ps in duration with additive white Gaussian noisy satellite pulses (see Fig. 1a) must be considered.

In the quasi-linear regime, at low intensity, the pulses undergo diffraction inside the crystal (see Fig. 1b). By increasing the incident intensity, the nonlinear self-focusing balances the effect of diffraction, as to the main signal; the noisy pulses behave linearly and undergo diffraction inside the crystal (see Fig. 1c).
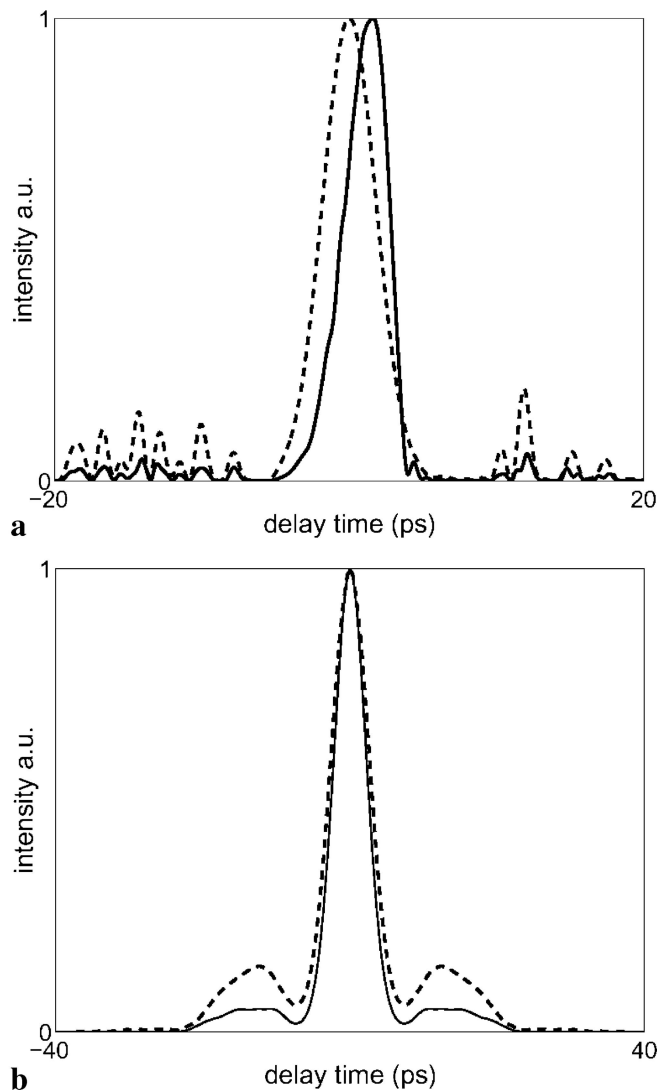


**FIGURE 2** FF temporal profiles (**a**) and temporal autocorrelation traces (**b**) at the input of the nonlinear medium (dashed line) and at the output of the spatial filter (continuous line). The phase-mismatch is $\Delta kL \sim 15\pi$, the input peak intensity is $I = 280\,\mathrm{MW/cm^2}$ and the slit width is equal to 0.9 times the input beam width
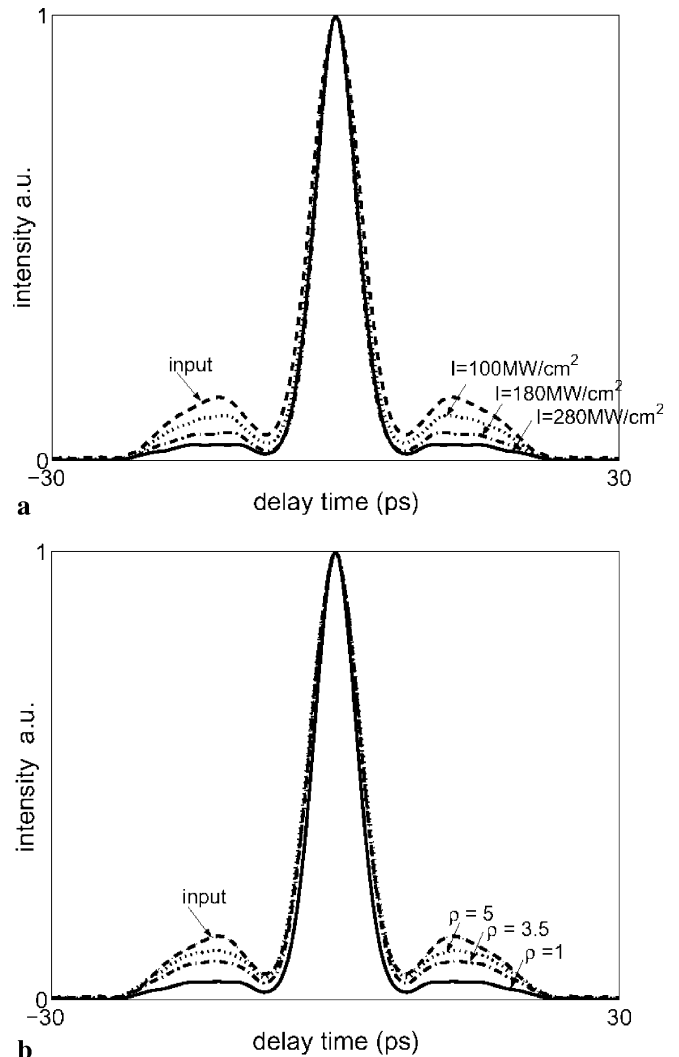


**FIGURE 3** **a** FF temporal autocorrelation traces at the output of the spatial filter, for different input peak intensities. The phase-mismatch is $\Delta kL \sim 15\pi$; the slit width was equal to 0.9 times the input beam width **b** FF temporal autocorrelation traces at the output of the spatial filter, for different values of $\varrho$ (slit aperture normalized to input beam width). The phase-mismatch is $\Delta kL \sim 15\pi$; the input peak intensity is $I = 280\,\mathrm{MW/cm^2}$

An aperture positioned at the output face of the nonlinear medium may block a consistent part of the non-trapped noisy energy and transmits the trapped beam. Typical numerical FF temporal beam profiles and temporal autocorrelation traces measured at the output of the spatial filter are, in self-trapped regime, superimposed to input temporal data are reported in Fig. 2.

The shaping mechanism is influenced both by the input intensity and by the spatial filter width. The input intensity, in fact, affects the characteristic width of the self-trapped beam and the behavior of the radiated field that can be blocked or not, according to the width of the spatial filter. FF numerical autocorrelation traces at the output of the spatial filter, varying the input intensity and the spatial filter width, are reported in Fig. 3.

The overall system, nonlinear propagation medium plus spatial filter, acts as a saturable absorber with an ultra-fast response time.

In the next section an experimental example of the all-optical nonlinear saturable absorber mechanism is shown.

## 3 Experimental

The experiments are performed with an all-fiber laser system delivering pulses at 1547 nm wavelength of about 3.9 ps (full width at half maximum) width and of 2 nm spectral bandwidth; the repetition rate is 20 MHz. The 58 mm long Ti : PPLN planar waveguide fabricated in a $Z$-cut substrate by indiffusion of a 70 nm thick, vacuum-deposited Ti-layer at 1060 °C. The micro domain structure of 16.92 μm periodicity has been generated by electric field assisted poling. The sample is inserted in a temperature stabilized oven and operated at elevated temperature (120–160 °C) to reduce photorefractive effects. By tuning the temperature it is possible to change the phase-matching conditions. The laser beam is shaped in a highly elliptical spot, nearly gaussian in profile, with full width at half maximum $w_{ox} = 56$ μm along the waveguide plane and $w_{oy} = 3.9$ μm along the perpendicular direction, for coupling to the guided mode. In this way a coupling efficiency of about 60% has been achieved. The spatial beam profiles at the output are recorded both with an IR camera and by a photodiode on a scanning system. Temporal measurements are performed with a non-collinear second harmonic generation autocorrelator. The spatial filtering is realized by a slit located in a plane where a magnified image of the output face of the crystal is displayed (Fig. 4).

The first experiment is devoted to the study of spatial trapping conditions. Because of the presence of a large temporal walk off, a spatial self-guided propagation is obtained only at large positive phase-mismatch between 148 °C ($\Delta kL \sim 7\pi$) and 110 °C ($\Delta kL \sim 58\pi$), limited by the available laser power. The temperature for perfect second harmonic generation phase matching is 154 °C. The evolution of the output beam size versus the input peak intensity at the FF permits to measure the trapping threshold to be about 200 MW/cm$^2$ (Fig. 5) at a temperature of 143 °C ($\Delta kL \sim 15\pi$). From that plot it can be deduced the intensity dependent transmission of the spatial filter with a width fixed at 0.9 times the input beam width. The calculation of the transmittance curve consists in the integration of the FF energy which falls in the slit aperture followed by a normalization to the total trapped energy. The transmission curve reaches a maximum of 90% for an intensity of 300 MW/cm$^2$, slightly above the trapping intensity threshold.
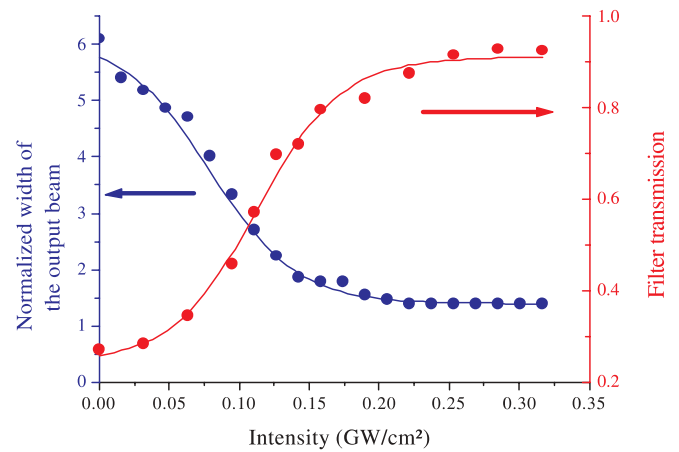


**FIGURE 5** Output beam size and transmittance of the system versus input peak intensity. The temperature was set at 143 °C ($\Delta kL \sim 15\pi$) and the slit width was equal to 0.9 times the input beam width
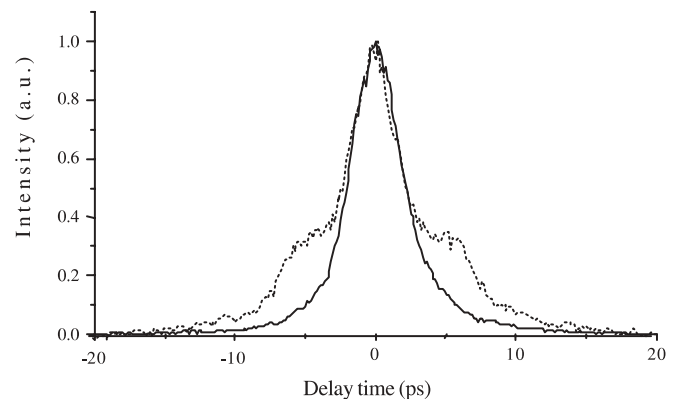


**FIGURE 6** Example of a temporal reshaping of picosecond pulses with a large modulation. Experimental data corresponding to the autocorrelation trace in the linear (*dashed line*) and in the soliton regime (*continuous line*) at the output of the spatial filter. The phase-mismatch was set at $\Delta kL \sim 15\pi$ with a slit width of 50 μm (0.9 times the input beam width) and a peak intensity of 326 MW/cm$^2$

In a second step the pulse reshaping produced by the set-up is considered. The adjustments of the laser system are changed so that it delivers laser pulses with trailing satellite pulses. The satellite signals are used as an example of distorted pulses and are launched into the waveguide. The temperature is set at 143 °C ($\Delta kl \sim 15\pi$) and a slit width close to the input beam size ($\sim 56$ μm) is chosen. In the linear regime, at low intensity, the recorded
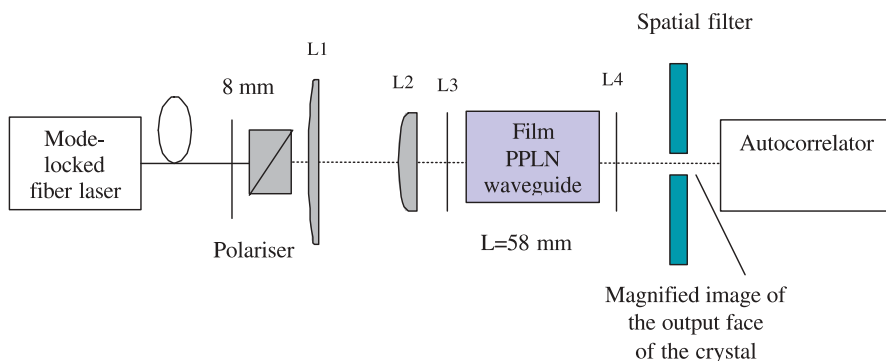


**FIGURE 4** Experimental set-up to investigate spatial self-trapping

autocorrelation trace exhibits a central Gaussian part of $\sim 6\,\mathrm{ps}$ with large shoulders. When the intensity is high enough to get self-trapping the pedestal in the trace are almost completely suppressed. Figure 6 compares the two situations.

To quantify the efficiency of the temporal filtering, we define a reshaping efficiency parameter $R_E$. The approach is based on the fact that in practice one wants to remove side lobes, tails and background noise from a main pulse usually of Gaussian shape. In the autocorrelation traces of the filtered pulses the fraction of energy is first calculated which is contained in a pure Gaussian distribution which fits the central part of the traces. The reshaping efficiency is equal to that contribution after normalisation to the total pulse energy.

In Fig. 7 the variation of the reshaping efficiency versus the input peak intensity for the input conditions mentioned above is plotted. The best filtering occurs at input intensities slightly higher than the self-trapping threshold ($250\,\mathrm{MW/cm^2}$). The data are recorded for a temperature of $143\,°\mathrm{C}$ ($\Delta kL \sim 15\pi$) and for a filter diameter equal to 0.9 times the spatial input width. At higher intensities the output beam profile starts to change slightly in comparison to the input profile: small side lobes grow and $R_E$ decreases.

The filtering efficiency depends also on the spatial filter width at the output of the nonlinear waveguide. For a slit wider than the output soliton width the shaping efficiency of the device is reduced. This is due to the fact, that also a fraction of the diffracted, low intensity wings of the input signal passes the filter. For an aperture narrower than the trapped beam width its most powerful central part only is transmitted, increasing $R_E$ in this way (Fig. 8). There is a trade-off between reshaping efficiency and transmitted power.

Due to the large group velocity mismatch a quasi-solitary wave can only be excited at sufficiently large positive phase mismatch ($\Delta kL > 7\pi$) (Fig. 9). Moreover, under the experimental conditions, an increase of the phase-mismatch corresponds to a decrease of the temperature which favours the parasitic influence of photorefractive effects and can reduce the reshaping efficiency.
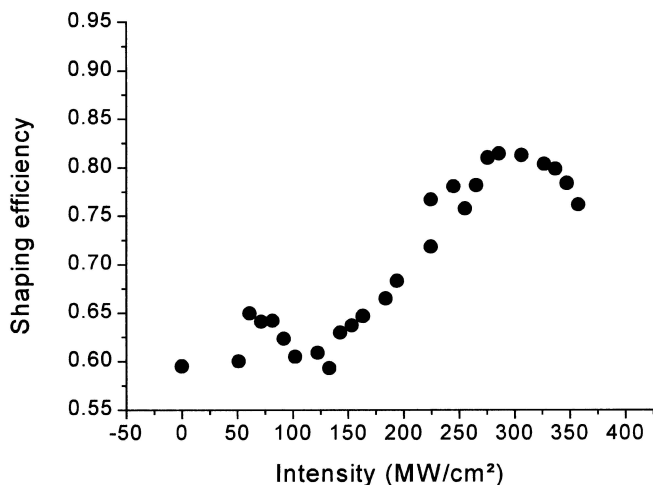


**FIGURE 8** Dependence of the shaping efficiency versus the normalised aperture. Here the input peak intensity is $346\,\mathrm{MW/cm^2}$ and the phase-mismatch is $\Delta kL \sim 15\pi$. The *dark line* is just a guide for the eye
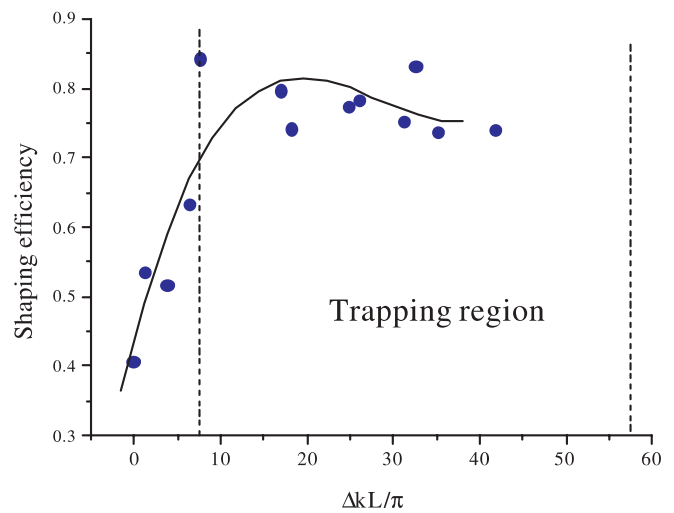


**FIGURE 9** Dependence of the shaping efficiency versus the phase-mismatch for an input peak intensity of $346\,\mathrm{MW/cm^2}$ and an aperture diameter of 0.9 times the input width (experiments). The *dark line* is just a guide for the eye

After the numerical and experimental demonstration of a temporal filtering of short pulses in PPLN waveguide, the device in question can be compared with other all-optical devices currently used in optical system with saturable absorber like action which are based on the Kerr effect in optical fiber. Intensity dependant polarization state through Kerr ellipse rotation or intensity dependant transmission with nonlinear optical loop mirror operate with lower energy. The high intensity required to reach spatial self trapping is clearly a drawback of the proposed nonlinear temporal filter. That issue could be overcome by the use of longer waveguide and/or the use of semiconductor nonlinear optical waveguide with larger second order nonlinearity (AlGaAs for example [19]). Film PPLN waveguides with engineered QPM offer also new opportunities to exploit soliton excitation and deflection at lower power [20].

Finally, it was already demonstrated that spatial trapping of a weak signal can be induced by a two color quadratic spatial soliton at a different wavelength [21]. Processing of weak



**FIGURE 7** Experimental data showing the dependence of the shaping efficiency versus incident peak intensity; here $\Delta kL \sim 15\pi$, the slit width is 0.9 times the input beam width
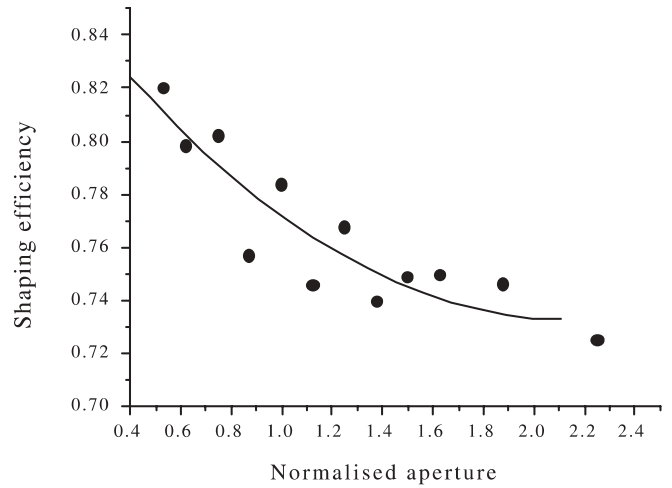
light signal is therefore achievable with this configuration by means of an internal source of command pulses carrying sufficient power. This device combines at the same time temporal reshaping of pulses and a retiming effect with respect to a clock signal.

## 4    Conclusions

It has been shown previously that the combination of self-trapped propagation in a second harmonic generation crystal with spatial filtering of the output beam worked as a saturable absorber. The initial experiments demonstrating the validity of the principle of operation were carried out at 1064 nm wavelength with 2D self-trapping in a KTP crystal. The method is adapted here to the wavelength range of optical communication: the input pulse wavelength is 1547 nm. To reduce the optical power required for "bleaching" the absorber, a Ti : PPLN film waveguide with the highest nonlinearity available today is used. Moreover, it is shown here that, despite the strong group velocity mismatch, the device can be operated even with picosecond pulses. Numerical simulations and experiments with distorted pulses of 4 ps width demonstrate that they can be significantly cleaned by passing the saturable absorber. The influence of various parameters on the efficiency of the pulse reshaping is characterised. From all the collected data it can be deduced that the best filtering occurs close to the soliton intensity threshold with a positive phase-mismatch slightly larger than the limit for self-trapping and for a spatial filter width slightly smaller than the input beam width. The study demonstrates that self-trapped propagation in a quadratic nonlinear waveguide can serve to build up an ultra-fast saturable absorber.

## REFERENCES

1  V.E. Zakharov, A.B. Shabat: Sov. Phys. JEPT **34**, 62 (1972)
2  A. Hasegawa, F. Tappert: Appl. Phys. Lett. **23**, 142 (1973)
3  L.F. Mollenauer, R.H. Stolen, J.P. Gordon: Phys. Rev. Lett. **45**, 1095 (1980)
4  A. Barthélémy, S. Maneuf, C. Froehly: Opt. Comm. **55**, 201 (1985)
5  J.S. Aitchison, A.M. Weiner, Y. Silberberg, M.K. Oliver, J.L. Jackel, D.E. Leaird, E.M. Vogel, P.W.E. Smith: Opt. Lett. **15**, 471 (1990)
6  A. Hasegawa, Y. Kodama: *Solitons in Optical Communications* (Clarendom 1995)
7  N.N. Akhmediev, A. Ankiewicz: *Soliton* (Chapman Hall, London 1997)
8  Y.N. Karamzin, A.P. Sukhorukov: Sov. Phys. JEPT **41**, 414 (1976)
9  W. Torruellas, Z. Wang, D.J. Hagan, E.W. Van Stryland, G.I. Stegeman, L. Torner, C.R. Menyuk: Phys. Rev. Lett. **74**, 5036 (1995)
10  M.D. Iturbe-Castillo, P.A. Marquez-Aguilar, J.J. Sanchez-Mondragon, S. Stepanov, V. Vysloukh: Appl. Phys. Lett. **64**, 408 (1994)
11  B. Bourliaguet, V. Couderc, A. Barthelemy, G. Ross, P.R. Smith, D.C. Hanna, C. De Angelis: Opt. Lett. **24**, 1410 (1999)
12  G. Leo, G. Assanto, W.E. Torruellas: Opt. Lett. **22**, 7 (1997)
13  B. Costantini, C. De Angelis, A. Barthelemy, B. Bourliaguet V. Kermene: Opt. Lett. **23**, 424 (1998)
14  A.V. Buryak, V.V. Steblina: J. Opt. Soc. Am. B. **16**, 245 (1999)
15  C. Simos, V. Couderc, A. Barthélémy: IEEE Phot. Tech. Lett. **14**, 636 (2002)
16  S. Carrasco, J.P. Torres, D. Artigas, L. Torner: Opt. Comm. **192**, 347 (2001)
17  P. Pioger, V. Couderc, L. Lefort, A. Barthelemy, F. Baronio, C. De Angelis, Y. Min, V. Quiring, W. Sohler: Opt. Lett. **27**, 2182 (2002)
18  L. Torner, G. Stegeman: J. Opt. Soc. Am. B. **14**, 3127 (1997)
19  S.J.B. Yoo, R. Bhat, C. Caneau, M.A. Koza: Appl. Phys. Lett. **65**, 3410 (1995)
20  F. Baronio, C. De Angelis: IEEE J. Quantum Electron. **QE-38**, 1309 (2002)
21  V. Couderc, E. Lopez Lago, C. De Angelis, F. Gringoli, A. Barthélémy: Optics communications **203**, 421 (2002)